sciendo

Acta Materialia Transylvanica 3/1. (2020) 26–32.
DOI: hungarian: https://doi.org/10.33923/amt-2020-01-05
english: https://doi.org/10.33924/amt-2020-01-05

ACTA MATERIALIA TRANSYLVANICA

Evaluation of Closed and Open-cell Structural Lattices with Finite Element Analysis

Klaudia KULCSÁR,[1] János KÓNYA [2]

Dent-Art-Technik Kft. Győr, Hungary

[1] *kulcsar.klaudia@dentarttechnik.hu*

[2] *janos@dentarttechnik.hu*

Abstract

Four lattice structures based on well-known crystal structures were evaluated in this study using the finite element method. Simple cubic, face-centered cubic, body-centered cubic, and diamond structural alignments were used to build up lattices from the body volume. Modern-day implant development trends are shifting towards additive manufacturing technologies, which have the advantage of creating structures that can improve the biological stability of implants that have integrated scaffolds. Such scaffolds can be trabecular structures that mimic bone tissue and facilitate tissue penetration into the porous parts of the implant. The final purpose of our study is to create an implant system that promotes the process of osseointegration. Evaluations have been carried out using finite element analysis.

Keywords*: closed cell structures, open cell structures, finite element analysis, crystal structures .*

1. Introduction

In orthopaedic surgery, cellular lattices are used as three-dimensional porous bio-products that attempt to mimic the structure and behaviour of bone tissue [1]. Porous biomaterial, which must be designed to have the same mechanical properties as that of bone tissue, may be used as bone replacements. Several other design factors that improve bone growth shall be considered as well. For example, permeability of the bone mimicking porous structure can affect cell migration [2]. Several principles have emerged in the last two decades allowing design structures that could replace bone tissue. These principles consider both mechanical properties, biocompatibility and bio functionality [3, 4]. In most studies, porous structures were made from titanium or titanium alloys, but titanium alloys are stiffer, and their mechanical properties outperform those of bone tissue [5]. Differences in mechanical properties of bone and titanium alloys can block bone growth and can cause bone resorption, which may lead to implant loosening [6, 7]. Porous structures are created with additive manufacturing technology, and their mechanical properties are closer to that of human bone [5, 8, 9].

In recent years, additive manufacturing technology (which some literature sources call rapid prototyping or 3D printing) has become widely popular. Here, the final product is made up layer-by-layer [10]. Selective Laser Melting (SLM) has been successfully developed recently to process metal powders. The density of parts manufactured with SLM can exceed 99 % [11]. Commercially pure titanium and titanium alloys are still generally used in medical implants to replace hard tissues and bone, because they have outstanding mechanical and biological properties [12]. Implants are also made from other biocompatible materials such as Co-Cr alloy and stainless steel. Comparing their elastic moduli with that of titanium alloys, one can see that the latter has a lower modulus of elasticity. However, elastic modulus of titanium is still much higher than that of human bone tissue [13]. Ahmadi et al studied six different lattice structures that had been manufactured with selective laser melting

(SLM) from Ti-6Al-4V ELI (Grade 23) powder. The types of studied lattice structures were simple cubic, diamond, truncated cube, truncated cuboctahedron, rhombic dodecahedron, and rombicuboctahedron. Cylindrical test specimens were manufactured using these previously mentioned structures. Then, they were subjected to static compression testing [14]. Chen et al studied open-cell models with different porosities. During their investigation, they studied the differences in the geometry of the porous structures between CAD models and final 3D printed parts. For example, the CAD model with 80 % theoretical porosity was printed with only 71 % porosity in practice [15].

2. Presentation of evaluated structures

The main purpose of this study was to create a porous scaffold that promotes and speeds up the osseointegration process at the bone-implant interface after implant insertion. In our previous studies, we experimented with 20×20 mm cubes that had been designed based on existing crystal structures. In this study, we investigated the environment of these small cubic structures by building up 60×60×60 mm cubes from them.

2.1. Simple cubic structure

Simple cubic structure was made up of 20×20×20 mm cubes with cutout spheres located at the corner points. Cutout sphere diameter was gradually increased in 0.1 mm increments. Figure 1 shows the phases of volume reduction. The lattice structure was designed as the negative of the crystal structure. The upper surface was left intact as a plane; no spheres were removed from there. Volume reduction was achieved by increasing cutout sphere diameter. For simple cubic structure, the closed-cell structure did not transform into an open-cell lattice. Thus, low volume reduction could be achieved in this case.

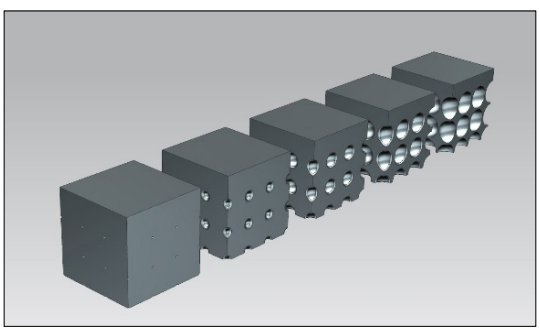

Figure 1. *Simple cubic cell structure from the solid model.*

2.2. Face-centered cubic structure

In face-centered cubic structure, cutout spheres were located at the cornerpoints and at the centre of each side of the cube. The upper surface was left intact as a plane; no spheres were removed from the cornerpoints. The porous structure was designed as the negative of the crystal structure. Figure 2 shows phases of volume reduction for face-centered cubic structure. For this structural alignment, it was observed that an open-cell structure emerged. Thus, large volume reduction could be achieved. Cutout sphere diameters were increased in 0.1 mm increments here as well.

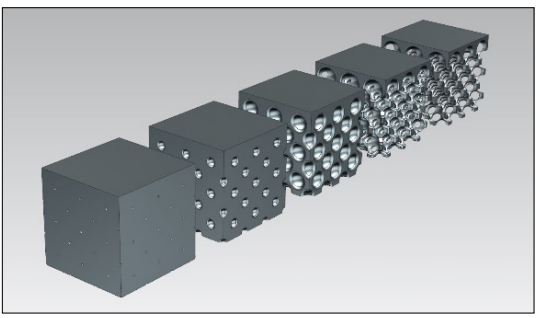

Figure 2. *Face-centered cubic structure from the solid model.*

2.3. Body-centered cubic structure

In body-centered cubic structural alignment, cutout spheres were located at the cornerpoints and at the middle of the body diagonal of the 20×20×20 mm cubes. For this solution, the upper surface was left planar as well, because no spheres were removed from those cornerpoints. The lattice was designed as the negative of the crystal structure. Cutout sphere diameter was increased in 0.1 mm increments here as well. Figure 3 shows phases of volume reduction for body-centered cubic structure. It is notable here that the structure transformed into an open-cell scaffold. Thus, large volume reduction could be achieved.

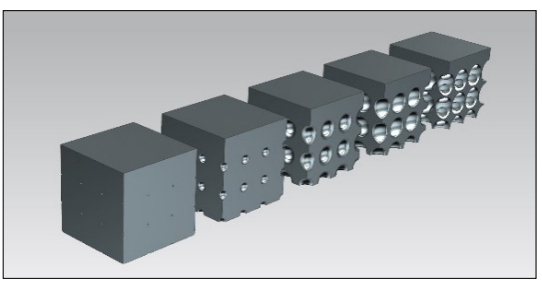

Figure 3. *Body-centered cubic structure from the solid body.*

2.4. Diamond structure

Diamond structure can be derived from face-centered cubic structure. This meant, cut-out spheres were located at the cornerpoints, at each side of the small cubes, and at the mid-octan centres as well. The upper surface was left planar here also. Thus, spheres were not removed from one mid-octan centre and from the upper cornerpoints of the cubes. Cutout sphere diameter was increased by 0.1 mm also. **Figure 4** shows phases of volume reduction for diamond structure.

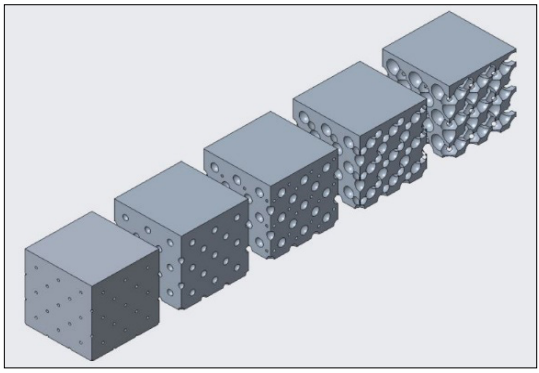

Figure 4. *Diamond structure from the solid body.*

3. Results of finite element analysis

Simulations were carried out using ANSYS software. For each of the above-mentioned structures, a 60×60×60 mm cube was created that consisted of smaller, 20×20×20 mm cubes. Mechanical loads were identical in all cases: the lower part of the cube was fixed, and 4500 N force was exerted on the upper planar surface. The acting force was evenly distributed, and a friction-free fix constraint was chosen. Stress intensity levels were analysed first, and can be seen in **Figure 5** on a representative meshed part.

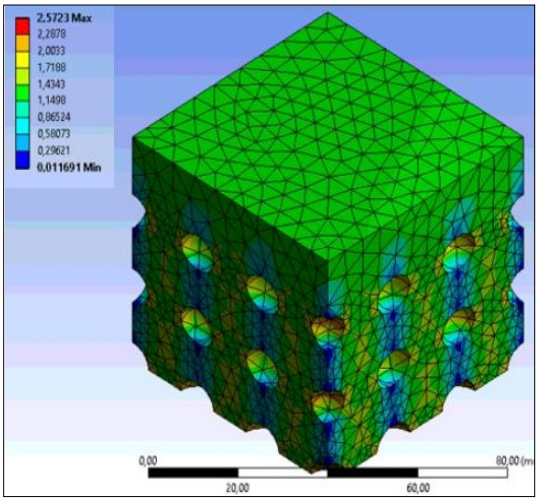

Figure 5. *Visualization of equivalent stress in the entire body.*

We wanted to see how the small cube in the centre behaves with its entire environment. Thus, stress intensity levels were analysed in the central small cube separately, too. One example is shown in **Figure 6** with its meshing.

Results of different structures were compared and then, stress intensity levels were compared in the entire body in order to find which structure provided the best results.

3.1. Results of simple cubic structure modelling

199 simulations were conducted on the part with simple cubic structure. The smallest cutout sphere diameter was 0.1 mm, while the largest was 19.9 mm. **Figure 7** shows measurement results. Maximum of equivalent stresses in the entire body and that in the central area were quasi identical. The lowest possible cell volume ratio, which is the ratio between the volume of the given lattice structure and the volume of the solid starting body in the form of a percentage, was only around 57 %. Equivalent stress levels were minimal here. The simple cubic structure was only a closed-cell scaffold.

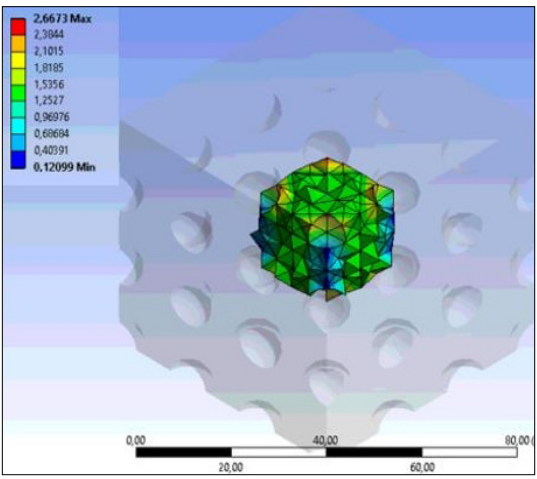

Figure 6. *Visualization of equivalent stresses in the centric cube.*

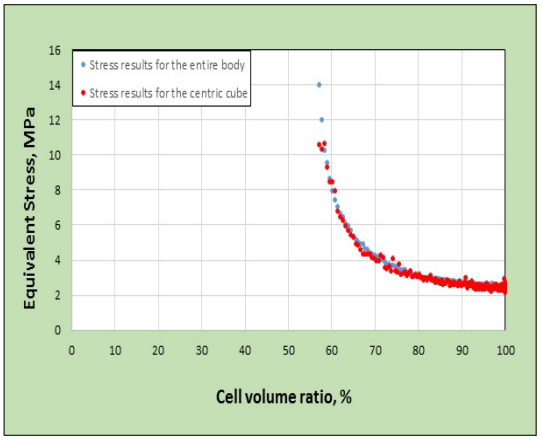

Figure 7. *Equivalent stress levels versus cell volume ratio in the parts with simple cubic lattice structure.*

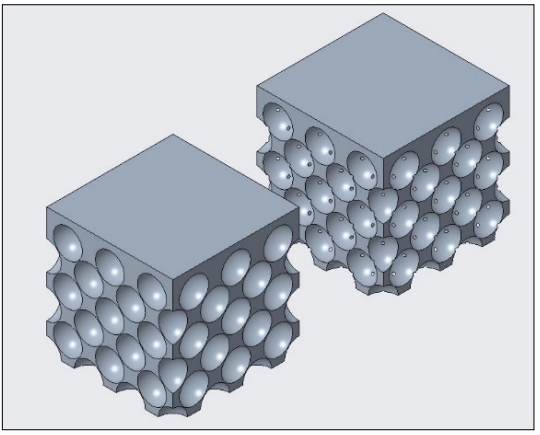

Figure 9. *Closed and open-cell structural geometry with face-centered cubic configuration.*

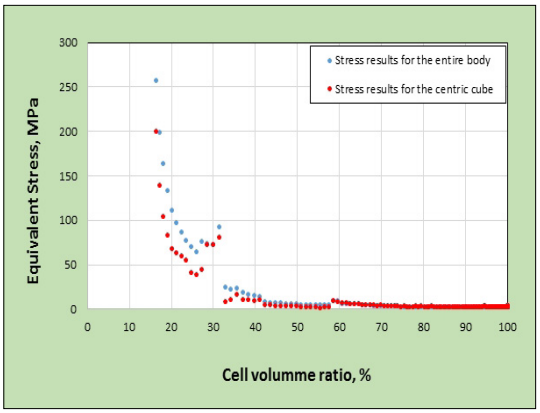

Figure 8. *Equivalent stress levels versus cell volume ratio in the parts with face-centered cubic lattice structure.*

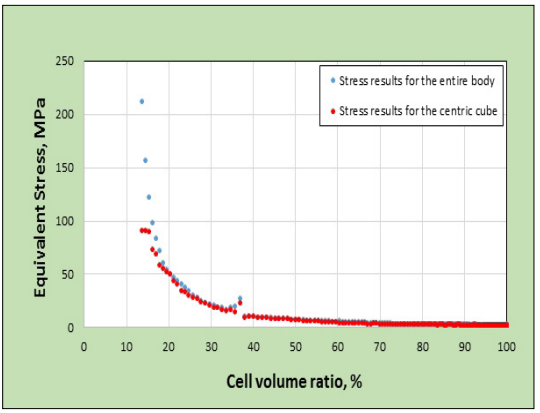

Figure 10. *Equivalent stress levels versus cell volume ratio in the parts with body-centered cubic lattice structure.*

3.2. Results of face-centered cubic structure modelling

155 simulations were conducted for face-centered cubic structure. The smallest diameter was 0.1 mm, while the diameter of the largest cutout sphere was 15.5 mm. **Figure 8** shows equivalent stress maximum levels for the part with face-centered cubic structure. At the volume ratio of 32 %, equivalent stress was higher. At that point, the lattice transformed from closed-cell to open-cell structure. Volume could be reduced substantially for the lattice with face-centered cubic structure, and stress intensity levels were still acceptable at the cell volume ratio of 20 %.

At te cell volume ratio of 32 %, the lattice transitioned from closed to open-cell configuration. **Figure 9** shows the geometries of the closed and open-cell structures.

3.3. Results of body-centered cubic structure modelling

199 simulations were conducted for body-centered cubic lattice structure with the smallest cutout sphere diameter of 0.1 mm. The largest removed spheres were 19.9 millimetres in diameter. **Figure 10** shows maximum equivalent stress levels for body-centered cubic lattice structure. Higher equivalent stress was measured at the volume ratio of 36 %. Then stress levels started to decrease and then increased again. This was the point where the closed-cell lattice transformed into an open-cell structure. Substantial volume reduction could be achieved for body-centered cubic structure, and equivalent stress levels were still considered particularly good at the cell volume ratio of 13 %.

At the cell volume ratio of 36 %, the structure transitioned from closed to open-cell configuration. Figure 11 shows the geometries of the closed and open-cell structures.

3.4. Results of diamond structure modelling

132 simulations were conducted for diamond lattice structure with the smallest cutout sphere diameter of 0.1 mm. The largest removed spheres were 13.3 millimetres in diameter. Figure 12 shows maximum equivalent stresses. Stress levels increased at the cell volume ratio of 63 %. It was the point when the closed-cell alignment transitioned into an open-cell one. There is another increase at 57 %. Equivalent stress levels for diamond lattice structure were acceptable up to the cell volume ratio of 40 %.

Figure 13 presents the geometric alignment of the closed and open-cell lattice structures. It is notable that this structure had more transition levels compared to the previously mentioned ones.

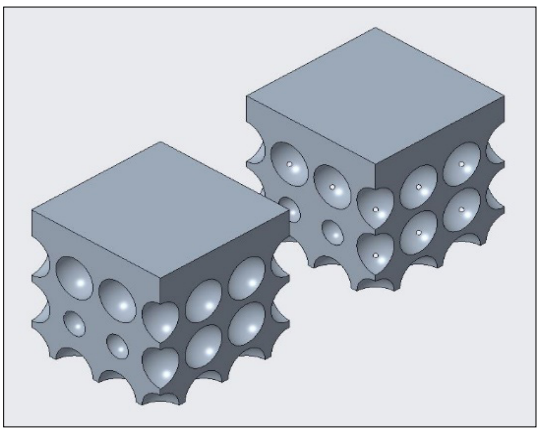

Figure 11. *Closed and open-cell structural geometry with body-centered cubic configuration.*

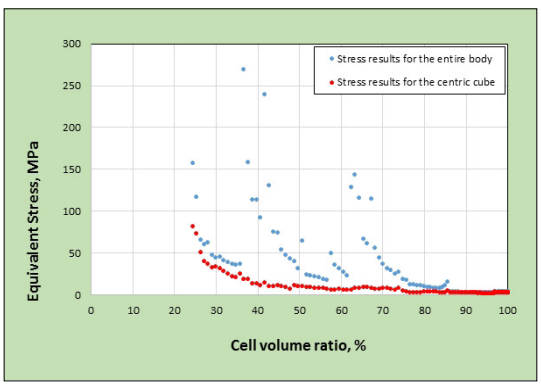

Figure 12. *Equivalent stress levels versus cell volume ratio in the parts with diamond lattice structure.*

4. Conclusions

Previously mentioned test results were collected in Figure 14. The diagram shows the sets of result points corresponding equivalent stress levels of the entire lattice for simple cubic, face-centered cubic, body-centered cubic, and diamond structures as a function of cell volume ratio. The least volume reduction could be achieved with the simple cubic structure type, so it is unimportant that stress results were low as well. This lattice remained a closed-cell structure “only”, which is why this solution can be considered irrelevant. Depending on the cell volume fraction, equivalent stress levels were higher for the diamond lattice structure. Face-centered and body-centered cubic lattice structures provided almost identical results up until the volume fraction of 35 %. Then, below this value, equivalent stress levels in the face-centered structure started to increase. Face-centered and body-centered cubic, and diamond structures could all contain closed and open-cell scaffolds. For all the three lattices, the transition from closed to open-cell structure was clearly noticeable. Increase in equivalent stress levels was well-defined, which was due to the reduced wall thicknesses in the solid models when structures transitioned from closed-cell to open-cell designs.

In this study, different cell structures were investigated that conformed to the atomic alignment of cubic crystal lattice structures. Equivalent stress levels were investigated both in the entire lattice and in its central area. To summarize, body-centered cubic lattice structure provided the best results. Calculations are going to be validated empirically as well on additively manufactured test specimens

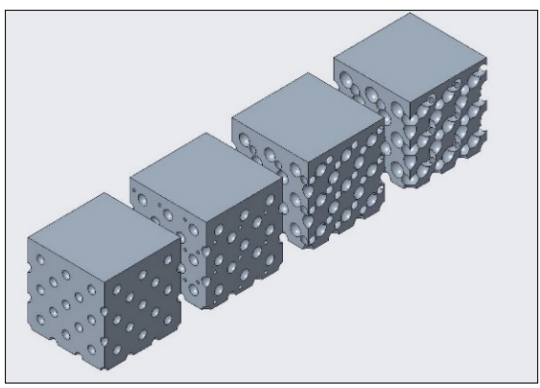

Figure 13. *Closed and open-cell structural geometry with diamond configuration.*

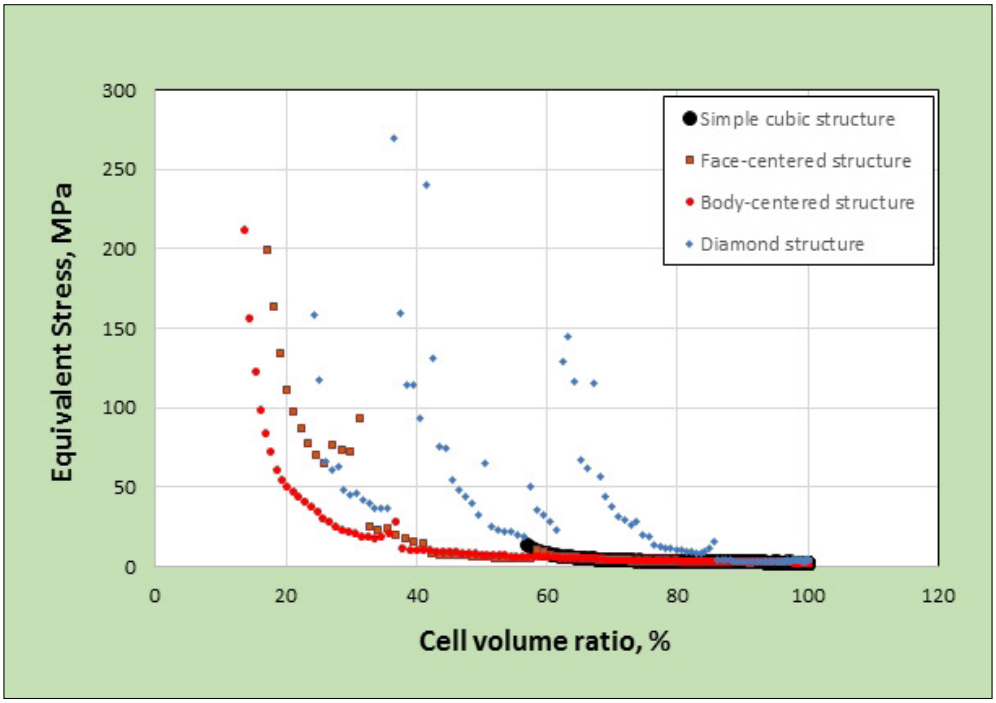

Figure 14. *Antegrated set of results.*

Acknowledgement

I would like to express my special thanks to János Dobránszky DSc, who helped in this study.

References

[1] Butscher A., Bohner M., Hofmann S., Gauckler L., Müller R.: *Structural and material approaches to bone tissue engineering in powder-based three-dimensional printing*. Acta Biomaterialia, 7/3. (2011) 907–920. https://doi.org/10.1016/j.actbio.2010.09.039

[2] Hollister S. J.: *Porous scaffold design for tissue engineering*. Nature Materials, 5/7. (2005) 518–524. http://doi.org/10.1038/nmat1421

[3] Hutmacher D. W.: *Scaffold design and fabrication technologies for engineering tissues – state of the art and future prespectives*. Journal of Biomaterials Science, Polymer Edition, 12/1. (2001) 107–124. https://doi.org/10.1163/156856201744489

[4] Goulet R. W., Goldstein S. S., Ciarelli M. J. et al.: *The relationship between the structural and orthogonal compressive properties of trabecular bone*. Journal of Biomechanics, 7/4. (1994) 379–389. https://doi.org/10.1016/0021-9290(94)90014-0

[5] Ahmadi S. M., Campoli G., Yavari S. A. et al.: *Mechanical behavior of regular open-cell porous biomaterials made of diamond lattice unit cells*. Journal of the Mechanical Behavior of Biomedical Materials, 34/1. (2014) 106–115. https://doi.org/10.1016/j.jmbbm.2014.02.003

[6] Engh C. A., Bobyn J. D., Glassman A. H.: *Porous-coated hip replacement. The factors governing bone ingrowth, stress shielding, and clinical results*. The Journal of Bone and Joint Surgery, 69-B/1. (1987) 45–55. https://doi.org/10.1302/0301-620X.69B1.3818732

[7] Huiskes R., Weinans H., van Rietbergen B.: *The relationship between stress shielding and bone resorption around total hip stems and the effects of flexible materials*. Clinical orthopaedics and related research, 274/1. (1992) 124–134. https://doi.org/10.1097/00003086-199201000-00014

[8] Amin Yavari S., Ahmadi S. M., van der Stock J. et al.: *Effects of bio-functionalizing surface treatments on the mechanical behavior of open porous titanium biomaterials*. Journal of the Mechanical Behavior of Biomedical Materials, 36/1. (2014) 109–119. https://doi.org/10.1016/j.jmbbm.2014.04.010

[9] Van der Stock J., Van der Jagt O. P., Amin Yavari S., et al.: *Selective laser melting-produced porous titanium scaffolds regenerate bone in critical size cortical bone defects*. Journal of Orthopaedic Research, 31/5. (2013) 792–799. https://doi.org/10.1002/jor.22293

[10] Gibson I., Rosen D. W., Stuckre B.: *Additive Manufacturing Technologies. Rapid Prototyping to Direct Digital Manufacturing*. Springer, New York, 2010. 6–9.

[11] Vandebroucke B., Kruth J. P.: *Selective laser melting of biocompatible metals for rapid manufacturing of medical parts*. Rapid Prototyping Journal, 13/4. (2007) 196–203. https://doi.org/10.1108/13552540710776142

[12] Li Y., Yang C., Zhao H. et al.: *New Developments if Ti-Based Alloys for Biomedical Applications*. Materials, 7/3. (2014) 1709–1800. https://doi.org/10.3390/ma7031709

[13] Zysset P. K., Guo X. E., Hoffler C. E.: *Elastic modulus and hardness of cortical and trabecular bone lamellae measured by nanoindentation in the human femur*. Journal of Biomechanics, 32/10. (1999) 1005–1012. https://doi.org/10.1016/S0021-9290(99)00111-6

[14] Ahmaid S. M., Yavari S. A., Wauthle R.: *Additively Maufactured Open-Cell Porous Biomaterials Made from Six Different Space-Filling unit Cells: The Mechanical and Morphological Properties*. Materials, 8/4. (2015) 1871–1896. https://doi.org/ 10.3390/ma8041871

[15] Chen S. Y., Huang J. C., Pan C. T.: *Microstructure and mechanical properties of open-cell porous Ti-6Al-4V fabricated by selective laser melting*. Journal of Alloys and Compounds, 713. (2017) 248–254. https://doi.org/10.1016/j.jallcom.2017.04.190